

Supporting Information

Solvent-free synthesis of a naphthoquinone-based bipolar organic cathode towards practical durable lithium organic battery

Jiakui Xiong^[a, b], Xiaorong Yan^[b, c], Haiping Yu^[b, d], Chuanguang Wu^[c], Guoqing Zhao^[b, c], Jianze Zhang^[a, b], Yujie Dai^[b, d], Xinyu Wang^[b, d], Jiefeng Gao^[f], Xiong Pu^[a, b, d], Mingjun Hu^{[b, c]*}, Jingru Liu^{[b, d]*}, Jun Yang^{[b, d, e]*}

[a] J. Xiong, J. Zhang, Prof. X. Pu

School of Chemistry and Chemical Engineering, Guangxi University
Nanning, 530004, China.

[b] J. Xiong, X. Yan, H. Yu, G. Zhao, J. Zhang, Y. Dai, X. Wang, Dr. M. Hu, Dr. J. Liu, Prof. X. Pu, Prof. J. Yang

Beijing Institute of Nano energy and Nano systems, Chinese Academy of Sciences
Beijing, 101400, China.
E-mail: yangjun@binn.cas.cn

[c] X. Yan, G. Zhao, Dr. C. Wu, Dr. M, Hu

School of Materials Science and Engineering, Beihang University
Beijing, 100191, China.
E-mail: mingjunhu@buaa.edu.cn

[d] H. Yu, Y. Dai, X. Wang, Dr. J. Liu, Prof. X. Pu, Prof. J. Yang

School of Nanoscience and Technology, University of Chinese Academy of Sciences
Beijing, 100049, China.

[e] Prof. J. Yang

Shensi Lab, Shenzhen Institute for Advanced Study, University of Electronic Science and Technology of China,
Longhua District, Shenzhen 518110, China.

[f] Prof. J. Gao

School of Chemistry and Chemical Engineering, Yangzhou University,
Yangzhou 225002, China

1 Experimental Section

1.1 DNQPA was synthesized by solvent-free method

All reagents were purchased without further processing. The 2-chloro-1,4-quinone (4 mmol, 98%, Macklin) and p-phenylenediamine (2 mmol, 99%, Macklin) were mixed thoroughly in a mortar. The mixture was then heated at 160°C under Ar for

8 h. After cooling to room temperature, it was washed with anhydrous ethanol. Finally, the product was dried under vacuum at 80 °C for 12 h. The yield was 66.7%.

1.2 DNQPA was synthesized by solvent method

A solution of 2-chloro-1,4-quinone (4 mmol, 98%, Macklin) in ethanol (30 ml) was charged in a 100 ml double-necked flask, and a solution of p-phenylenediamine (2 mmol, 98%, Macklin) dissolved in 30 ml ethanol was added slowly using a constant pressure dropping funnel for more than 15 min. After mixing the reagents, the reaction solution was stirred at room temperature for 24 h. Then the brown precipitate was filtered and washed with ethanol. Finally, the product was dried under vacuum at 80°C for 12h with a yield of 32.6%.

1.3 The synthesis of D/G-x

Take D/G-50% as an example. 15 mg DNQPA and 30 mg reduced graphene oxide were put into a small glass vial, and 8 ml anhydrous ethanol was added and sonicated for 6 h. After drying under vacuum at 80 °C for 48 h, the complex D/G-50% was obtained. (Other D/G-x composites were synthesized in the same way with D/G-50% but with different D/G mass ratios).

1.4 The synthesis of NQ/G

The NQ/G was synthesized in the same way with D/G-50%. 15 mg NQ and 30 mg reduced graphene oxide were put into a small glass vial, and 8 ml anhydrous ethanol was added and sonicated for 6 h. After drying under vacuum at 80 °C for 48 h, the complex NQ/G was obtained.

1.5 Materials characterizations

The pure products were ground into powder for characterization. The crystalline structure of DNQPA and composites was described using X-ray powder

diffractometer (Bruker D8 ADVANCE) by Cu K α radiation source. The scanning rate was 0.2°min⁻¹, and the scanning range was 5° to 60°. The molecular weight of DNQPA was verified using liquid chromatogram coupled (Waters ACQUITY UPLC I-Class PLUS) with mass spectrometer (Waters Xevo G2-XS QTof). First, the product was soaked in 2 mL of chromatographic methanol and dimethyl sulfoxide (4:1 v/v) mixture to dissolve the active substance in the solution. Then two drops of the solution using a 100 μ L pipette were added to an UPLC-MS vial with 1 mL additional chromatographic methanol. The samples were detected by ¹H nuclear magnetic resonance (NMR JNM-ECA600) and diluted with deuterated chloroform (CDCl₃) after dissolution. Fourier transform infrared spectroscopy (FTIR, Nicolet IS 10, USA) was performed using a single reflection ATR module with a scanning range of 400-4000 cm⁻¹. Thermogravimetric analysis (TGA) was used to test the thermal stability of the samples with a heating rate of 10°C/min from room temperature to 800°C under pure nitrogen atmosphere. The cathode composites were detected by Scanning electron microscopy (SEM) and energy dispersive spectrometry (EDS) using Carl Zeiss Sigma 500 field emission. The samples were sonicated and dispersed in anhydrous ethanol, then added dropwise onto silicon wafers, and finally dried at 60°C before testing.

1.6 Electrochemical measurements

The electrochemical performance of the samples was evaluated by assembling CR2032 coin cells in an argon (Ar)-filled glove box. First, the cathode slurry of DNQPA was prepared by mixing DNQPA, Super P and PVDF with the mass ratio of 6:3:1 in NMP. The slurry was coated on aluminum foil and dried overnight at 80 °C with the active materials loading of about 0.9 mg cm⁻² (the NQ cathode is prepared in the same way as the DNQPA cathode). Then a series of D/G-x cathodes

with different loadings were prepared according to the same method with a mass ratio of 9:1 between D/G-x and PVDF, and the active materials loadings are about 0.8-1.0 mg cm⁻² (the NQ/G cathode is prepared in the same way as the D/G-x cathode). Finally, lithium metal discs were used as anode, Celgard 2400 membrane was used as a septum and the electrolyte was 2 M lithium bis(trifluoromethane)sulfonimide (LiTFSI) dissolved in 1,3-dioxane/1,2-dimethoxyethane (DOL/DME, v/v = 1/1). Electrochemical measurements were performed after an equilibration time of 3 h. At room temperature, the galvanostatic charge/discharge measurements were performed on coin cells at various currents in the voltage range of 1.5-3.9 V using a LAND CT2001A. The charge/discharge specific capacity is determined based on the mass of active material in the electrodes. Cyclic voltammograms (CV) and electrochemical impedance spectra (EIS) were tested at the CHI604E electrochemical workstation. The cell was swept from the open-circuit voltage (OCV) to 4.0 V and then back to 1.5 V at different scan rates. CV was measured at scan rates of 0.6 mV s⁻¹, 0.8 mV s⁻¹, 1 mV s⁻¹, 1.2 mV s⁻¹ and 1.4 mV s⁻¹, respectively. The direct current voltage was kept at open-circuit voltage and an alternating current voltage of 5 mV in amplitude was applied with a frequency of 0.1 Hz-200 kHz was used to test the EIS.

1.7 The calculation of molecular electrostatic potential

The geometric optimization and frequency calculation of DNQPA and NQ were performed at B3LYP-D3(BJ)/6-31G(d), and the energy calculation of DNQPA and NQ use B3LYP-D3(BJ)/6-311G(d,p),^{1,2} level using Gaussian 9 program package.
²² The RDG and ESP calculation were analyzed using Multiwfn program,³ and the isosurface was visualized using VMD.⁴

2 Figures and Tables

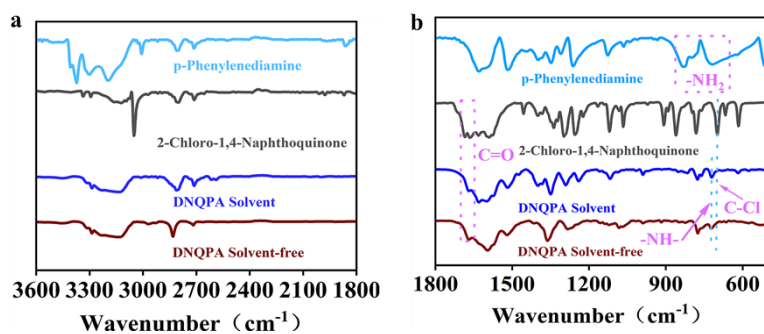


Figure S1. The FTIR spectra of the precursors, DNQPA-S and DNQPA-SF with wavenumber between (a) 3600–1800 cm^{-1} and (b) 1800–500 cm^{-1} .

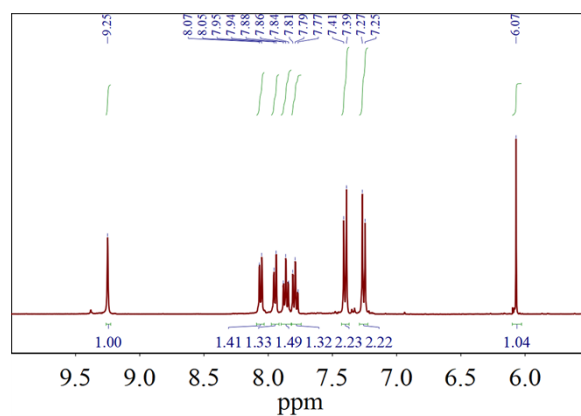


Figure S2. ¹H nuclear magnetic resonance (NMR) spectrum of DNQPA-S.

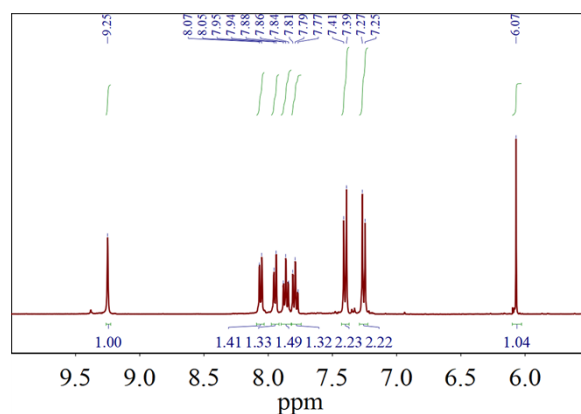


Figure S3. ¹H nuclear magnetic resonance (NMR) spectrum of DNQPA-SF.

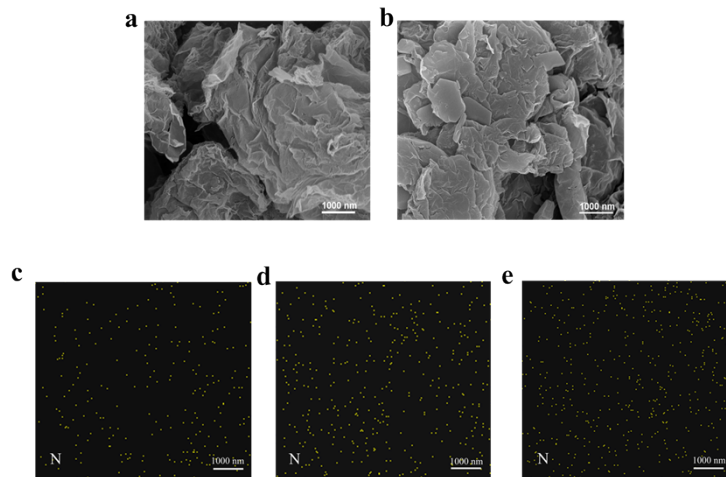


Figure S4. The SEM images of (a) D/G-30% and (b) D/G-80% composites. The SEM-EDS mapping of N elemental distributions on (c) D/G-30% composite, (d) D/G-50% and (e) D/G-80% composites.

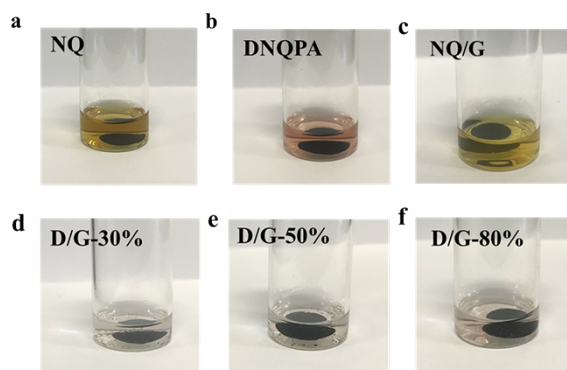


Figure S5. The solubility tests of (a) NQ, (b) DNQPA, (c) NQ/G, (d) D/G-30%, (e) D/G-50% and (f) D/G-80% electrodes after 72h (soaking in 1,2-dimethoxyethane (DME)).

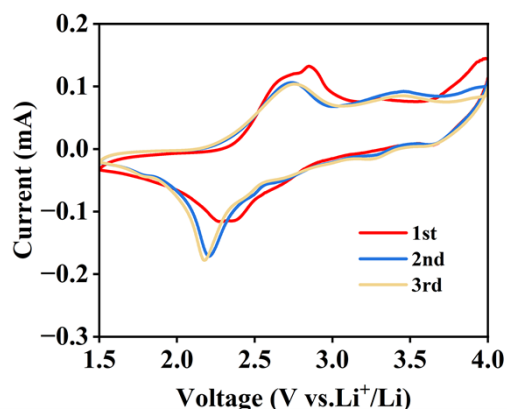


Figure S6. CV of DNQPA cathode in the range of 1.5–4.0 V and at scan rate of 3 mV s^{-1} .

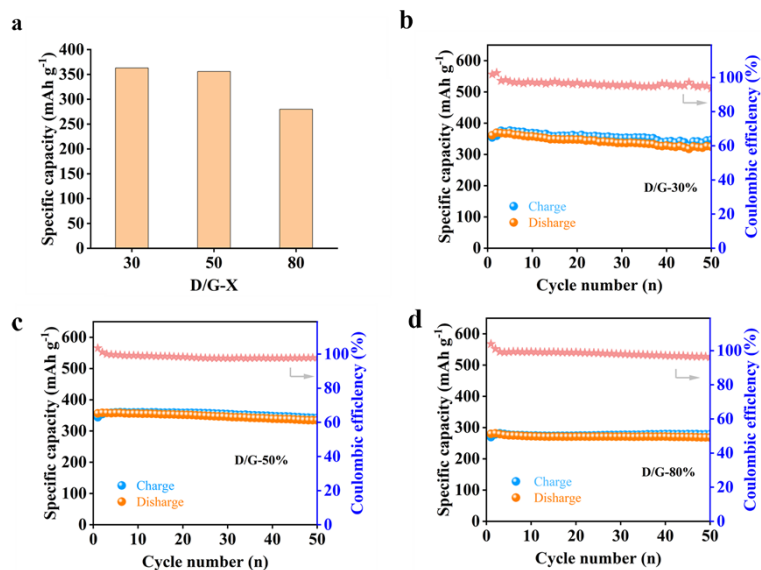


Figure S7. (a) Discharge capacity of D/G-x cathodes at a current density of 0.1 A g⁻¹. Cycling stability test of (b) D/G-30%, (c) D/G-50% and (d) D/G-80% for 50 cycles at 0.1 A g⁻¹.

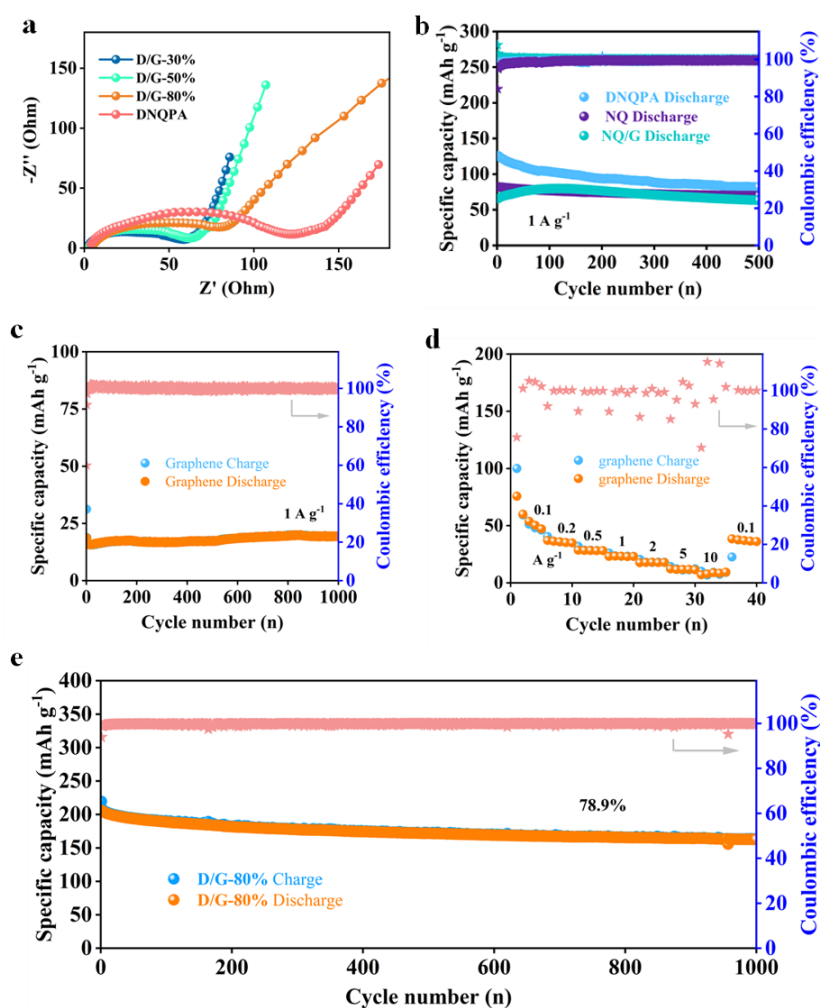


Figure S8. (a) Nyquist plots of D/G and DNQPA. (b) Cycling test of DNQPA, NQ and NQ/G for 500 cycles at 1 A g⁻¹. (c) Cycling performance of graphene and (e) D/G-80% for 1000 cycles at 1 A g⁻¹. (d) Rate performance of Graphene.

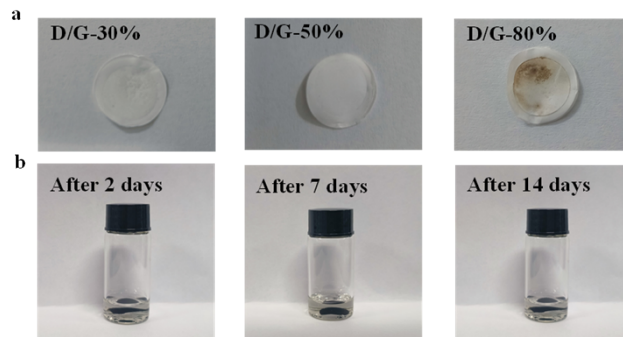


Figure S9. (a) The images of batteries with different electrodes after cycling for 200 cycles. (b) The solubility tests of D/G-50% electrode after 200 cycles (soaking in 1,2-dimethoxyethane (DME)).

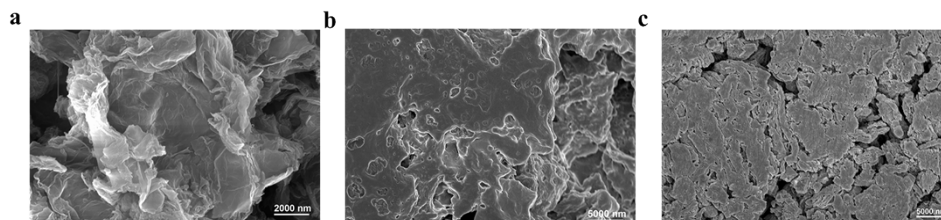
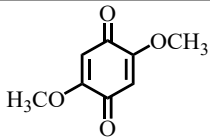
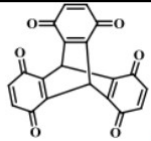
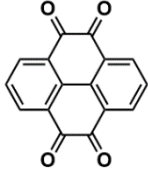
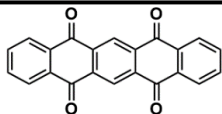
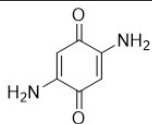
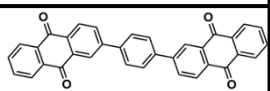
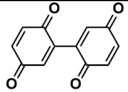
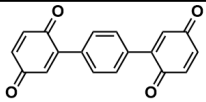
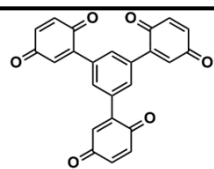
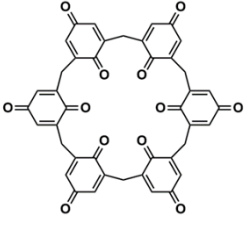
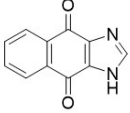
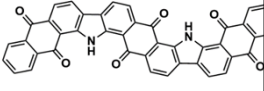
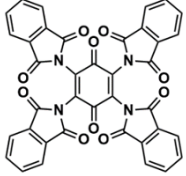
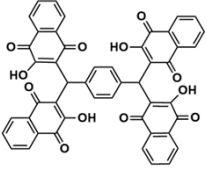
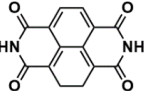
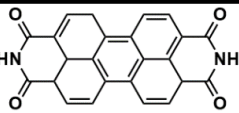
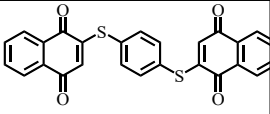
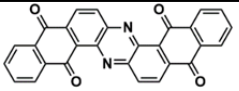
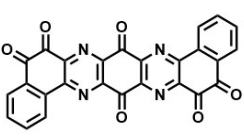
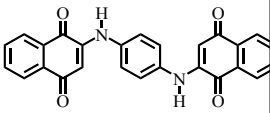
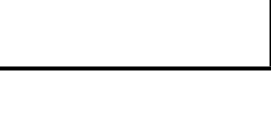


Figure S10. The SEM images of D/G-50% electrode, (a) before test, (b) after 50 cycles and (c) after 200 cycles.

Table S1. Comparison of the reported quinone-derived organic molecules as the cathode materials for lithium organic batteries. (S: large quinone-based molecules; G: quinone molecules composited with carbon materials; F: quinone molecules with multiple functional groups)

Number	Material	Final capacity (mA h g ⁻¹) @ current density	Cycle number	Capacity retention	Ref.
S1		255@20 mA g ⁻¹	10	80.1%	5
S2		224@1C	100	76.0%	6
S3		75.6 @20 mA g ⁻¹	50	21.0%	7
S4		184.08 @20 mA g ⁻¹	100	78.0%	8
G5		248.32@0.05C	15	64.4%	9
G6		195.6@ 44 mA g ⁻¹	100	91.0%	10
G7		149.43@38 mA g ⁻¹	100	51.0%	11
G8		306.3@37 mA g ⁻¹	100	83%	11
G9		218.35@41 mA g ⁻¹	100	55%	11

G10		272.79@ 45 mA g ⁻¹	300	63%	12
G11		152@0.2C	100	64%	13
F12		240.9@100 mA g ⁻¹	200	96.0%	14
F13		212@347 mA g ⁻¹	100	91%	15
F14		116.8@50 mA g ⁻¹	300	73%	16
F15		175 @ 1000 mA g ⁻¹	2000	81%	17
F16		123@100 mA g ⁻¹	200	97%	18
F17		181.39@5C	500	93.5%	19
F18		196.08@ 500 mA g ⁻¹	1000	76%	20
F19		303@100 mA g ⁻¹	100	83%	21
G20		258.1@1000mA g ⁻¹	1000	89.3%	This work
G21		215.8@5000mA g ⁻¹	9000	85.6%	This work

References

1. W. J. Hehre, R. Ditchfield and J. A. Pople, *The Journal of Chemical Physics*, 1972, **56**, 2257-2261.
2. P. C. Hariharan and J. A. Pople, *Theoretica chimica acta*, 1973, **28**, 213-222.
3. T. Lu and F. Chen, *J. Comput. Chem.*, 2012, **33**, 580-592.
4. W. Humphrey, A. Dalke and K. Schulten, *Journal of Molecular Graphics*, 1996, **14**, 33-38.
5. M. Yao, H. Senoh, S.-i. Yamazaki, Z. Siroma, T. Sakai and K. Yasuda, *J. Power Sources*, 2010, **195**, 8336-8340.
6. J. E. Kwon, C.-S. Hyun, Y. J. Ryu, J. Lee, D. J. Min, M. J. Park, B.-K. An and S. Y. Park, *J. Mater. Chem. A*, 2018, **6**, 3134-3140.
7. Y. Liang, P. Zhang and J. Chen, *Chem. Sci.*, 2013, **4**, 1330-1337.
8. M. Yao, S.-i. Yamazaki, H. Senoh, T. Sakai and T. Kiyobayashi, *Materials Science and Engineering: B*, 2012, **177**, 483-487.
9. L. Sieuw, A. Jouhara, É. Quarez, C. Auger, J.-F. Gohy, P. Poizot and A. Vlad, *Chem. Sci.*, 2019, **10**, 418-426.
10. J. Yang, H. Su, Z. Wang, P. Sun and Y. Xu, *ChemSusChem*, 2020, **13**, 2436-2442.
11. J. Yang, P. Xiong, Y. Shi, P. Sun, Z. Wang, Z. Chen and Y. Xu, *Adv. Funct. Mater.*, 2020, **30**, 1909597.
12. W. Huang, X. Zhang, S. Zheng, W. Zhou, J. Xie, Z. Yang and Q. Zhang, *Sci. China Mater.*, 2020, **63**, 339-346.
13. J. Lee, H. Kim and M. J. Park, *Chem. Mater.*, 2016, **28**, 2408-2416.
14. F. Men, N. Liu, Q. Lan, Y. Zhao, J. Qin, Z. Song and H. Zhan, *ChemSusChem*, 2020, **13**, 2410-2418.
15. Z. Luo, L. Liu, Q. Zhao, F. Li and J. Chen, *Angew. Chem. Int. Ed.*, 2017, **56**, 12561-12565.
16. M. Miroshnikov, K. Kato, G. Babu, N. Kumar, K. Mahankali, E. Hohenstein, H. Wang, S. Satapathy, D. K. P, H. Asare, P. Ajayan, L. Arava and G. John, *ACS Sustainable Chemistry & Engineering*, 2019, **7**, 13836-13844.
17. Y. Shi, H. Tang, S. Jiang, L. Kayser, M. Li, F. Liu, F. Ji, D. Lipomi, S. Ong and Z. Chen, *Chem. Mater.*, 2018, **30**, 3508-3517.
18. C. Peng, G.-H. Ning, J. Su, G. Zhong, W. Tang, B. Tian, C. Su, D. Yu, L. Zu, J. Yang, M.-F. Ng, Y.-S. Hu, Y. Yang, M. Armand and K. P. Loh, *Nat. Energy*, 2017, **2**, 17074.
19. B. Zhao, Y. Si, W. Guo and Y. Fu, *Adv. Funct. Mater.*, 2022, **32**, 2112225.
20. T. Shi, G. Li, Y. Han, Y. Gao, F. Wang, Z. Hu, T. Cai, J. Chu and Z. Song, *Energy Stor. Mater.*, 2022, **50**, 265-273.
21. Z. Chen, J. Wang, T. Cai, Z. Hu, J. Chu, F. Wang, X. Gan and Z. Song, *ACS Appl. Mater. Interfaces*, 2022, **14**, 27994-28003.
22. Gaussian 16, Revision A.03, M. J. Frisch, G. W. Trucks, H. B. Schlegel, G. E. Scuseria, M. A. Robb, J. R. Cheeseman, G. Scalmani, V. Barone, G. A. Petersson, H. Nakatsuji, X. Li, M. Caricato, A. V. Marenich, J. Bloino, B. G. Janesko, R. Gomperts, B. Mennucci, H. P. Hratchian, J. V. Ortiz, A. F. Izmaylov, J. L. Sonnenberg, D. Williams-Young, F. Ding, F. Lipparini, F. Egidi, J. Goings, B. Peng, A. Petrone, T. Henderson, D. Ranasinghe, V. G. Zakrzewski, J. Gao, N. Rega, G. Zheng, W. Liang, M. Hada, M. Ehara, K. Toyota, R. Fukuda, J. Hasegawa, M. Ishida, T. Nakajima, Y. Honda, O. Kitao, H. Nakai, T. Vreven, K. Throssell, J. A. Montgomery, Jr., J. E. Peralta, F. Ogliaro, M. J. Bearpark, J. J. Heyd, E. N.

Brothers, K. N. Kudin, V. N. Staroverov, T. A. Keith, R. Kobayashi, J. Normand, K. Raghavachari, A. P. Rendell, J. C. Burant, S. S. Iyengar, J. Tomasi, M. Cossi, J. M. Millam, M. Klene, C. Adamo, R. Cammi, J. W. Ochterski, R. L. Martin, K. Morokuma, O. Farkas, J. B. Foresman, D. J. Fox, Gaussian, Inc., Wallingford CT, 2016.